The "Cheerios effect"

Dominic Vella and L. Mahadevan[a)]
Division of Engineering and Applied Sciences, Harvard University, Pierce Hall, 29 Oxford Street, Cambridge, Massachusetts 02138

(Received 22 November 2004; accepted 25 February 2005)

Objects that float at the interface between a liquid and a gas interact because of interfacial deformation and the effect of gravity. We highlight the crucial role of buoyancy in this interaction, which, for small particles, prevails over the capillary suction that often is assumed to be the dominant effect. We emphasize this point using a simple classroom demonstration, and then derive the physical conditions leading to mutual attraction or repulsion. We also quantify the force of interaction in particular instances and present a simple dynamical model of this interaction. The results obtained from this model are validated by comparison to experimental results for the mutual attraction of two identical spherical particles. We consider some of the applications of the effect that can be found in nature and the laboratory. © *2005 American Association of Physics Teachers.*
[DOI: 10.1119/1.1898523]

I. INTRODUCTION

Bubbles trapped at the interface between a liquid and a gas rarely rest. Over a time scale of several seconds to minutes, long-lived bubbles move toward one another and, when contained, tend to drift toward the exterior walls (see Fig. 1). Readers may readily verify these claims by pouring themselves a glass of sparkling water and following the motion of those bubbles at the surface—particularly those at the periphery of the glass. This phenomenon has been affectionately dubbed the ''Cheerios effect'' after the observation that breakfast cereals floating in milk often clump together or stick to the walls of the breakfast bowl.[1]

In this article, we bring together a number of perspectives on the Cheerios effect gathered from the literature and our own experience at home, in the kitchen, and in the laboratory. We show how simple physical ideas lead to an understanding not only of the attraction, but also of its dynamical consequences. Despite being a subject with enormous potential for simple, reliable party tricks, the technological implications of the Cheerios effect are far from frivolous. Much research is currently being done to investigate the possibility of using surface tension to induce the self-assembly of small-scale structures.[2] Understanding the way in which particles aggregate at an interface, and hence being able to control the form of the aggregate as well as the dynamics of its formation, may one day enable much simplified manufacture of components of micro-electromechanical systems.

For floating objects in equilibrium, we must consider the balance of linear momentum both in the flotation plane as well as out of the plane, and in addition the balance of angular momentum in all three directions. Many of the misconceptions in the field arise from considering only some but not all of these balance equations. In particular, neglecting the condition of vertical force balance leads to an underestimation of the importance of the particle's buoyancy in determining the nature of the interaction.

We begin with a discussion of the physical mechanism that leads to the observed attraction in most instances and illustrate the role of particle buoyancy by a simple experiment. We then focus on a series of simple examples that allow us to quantify the magnitude of the attractive force. The first of these examples is inspired by an oversimplified physical picture that often is portrayed as a complete explanation of the Cheerios effect. By considering the vertical force balance that must be satisfied for particles to float, we will show that it is the effects of buoyancy that dominate for small particles and propose a simple dynamical model for the attraction of two spherical particles. Finally, we show that consideration of the remaining equilibrium condition, that of torque balance, can lead to amphiphilic strips. We conclude with some possible biological implications of our observations.

II. THE PHYSICAL ORIGIN OF ATTRACTION

The mechanism behind the apparent attraction between bubbles or between a bubble and the wall of a glass is easy to understand by considering the geometry of the interface at which the bubbles are trapped. For simplicity, we consider the latter case (schematically illustrated in Fig. 2), although the explanation of the clustering of many bubbles is similar. Here, the air–water interface is significantly distorted by the presence of the wall (the well-known meniscus effect), and because the bubble is buoyant, there is a net upward force due to gravity, F_g, on the bubble. Because it is constrained to lie at the interface, however, the bubble cannot simply rise vertically, and instead does the next best thing by moving upward *along* the meniscus. Because water wets glass (the contact angle θ defined in Fig. 2 satisfies $\theta < \pi/2$), in moving

Fig. 1. Bubbles floating on water in a petri dish. The bubbles are observed to aggregate before moving to the wall of the container. After sufficiently long times, the island of bubbles in the center also migrates to the wall.

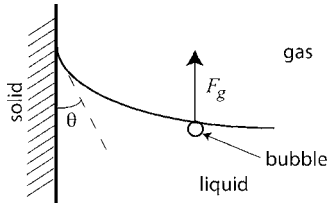

Fig. 2. Schematic of a single bubble close to a wall, along with the definition of the contact angle.

upward and along the meniscus the bubble also moves closer to the wall. Viewed from above, it appears as if there is an attractive force acting between the wall and the bubble when in fact the buoyancy of the bubble causes it to move in response to the curved meniscus.

A single bubble will deform the interface just as the presence of a wall does, although for a different reason and to a lesser extent. In the case of the bubble, it can only remain at the interface because the buoyancy force, which tends to push the bubble out of the liquid, is counterbalanced by the surface tension force, which opposes the deformation of the interface and hence acts to keep the bubble in the liquid. These two competing effects reach a compromise where the bubble is partially out of the liquid but the interface is slightly deformed. This deformation is sufficiently significant to influence other bubbles nearby, which move upward along the meniscus and so spontaneously aggregate.

This mechanism was first proposed by Nicolson[3] as a means by which the bubbles that constitute a bubble raft interact and give the raft its solid-like properties. As we shall see in Sec. V, this mechanism provides the dominant contribution for the interaction between sufficiently small particles.

The same argument works for floating particles that are significantly more dense than water. That such heavy particles can float at all is due to the fact that surface tension stops the interface from deforming too much downward as would happen if the particle were to sink. This reversal of the interfacial curvature can be seen clearly in Fig. 3 for a metal pin floating on water: surface tension must act upward to counterbalance the weight of the pin. In analogy with what is observed with bubbles, we would expect that another drawing pin floating near the first will "fall" down the interface, and hence the two appear to be attracted to one another, as is observed.

Fig. 3. A photograph of a drawing pin floating upturned on water. Notice that the deformation of the interface in this case is opposite to that around a bubble or near a wetting wall.

III. REPULSION: OFTEN MISUNDERSTOOD

So far we have seen that the deformation of an interface caused by the presence of particles at that interface can lead to mutual attraction between these particles and eventually to the formation of large clusters. We have seen, however, only one half of the story. Imagine that we were to float a buoyant bubble in the vicinity of a drawing pin–would they also attract? On the basis of the previous argument, we expect that the bubble will move upward along the interface distorted by the presence of the drawing pin. However, because the pin is not buoyant, that is, the interface has the curvature shown in Fig. 3, moving along the interface will, in this case, cause the bubble to move away from the drawing pin and so the two objects *repel* one another.

A more striking demonstration of this repulsion can be achieved using two drawing pins, provided they are the kind that has a thin plastic cap around the blunt end. As we would expect from the discussion given in Sec. II, these two drawing pins will attract when floated at the interface. However, if we now carefully remove the plastic cap from the top of one and float it (the cap) near the intact drawing pin, then the two will move apart.

This simple experiment apparently challenges the common assumption that the attraction or repulsion of particles at interfaces depends solely on the wetting properties, namely, the contact angles, of the particles (see, for example, Ref. 4, p. 70, example 3 or Ref. 5). Here, the wetting properties of the plastic cap (which is the only part that is in contact with the liquid) are not altered by removing it from the pin, but the weight that it must support is much reduced, making the cap buoyant. In turn, this buoyancy alters the balance between surface tension and gravity so that the interface must now pull down on the cap to keep it at the interface, and so the deformation near the cap resembles that around a bubble. This change in the sign of the curvature of the interface was brought about without changing the surface properties of the cap. Instead, it occurs simply because of a change in the effective density of the particle, which is a possibility that appears not to have been explored fully.[6]

IV. A MODEL CALCULATION

Quantifying the physical picture outlined in Sec. II allows us not only to predict the conditions under which the interfacial curvature changes sign, but also to understand simply the dynamical interaction between two particles. We start with an idealized problem in which we account only for the condition of horizontal force balance (and neglect the vertical force and torque balance conditions) by focusing on two infinite vertical plates at a liquid–gas interface, as shown in Fig. 4. The presence of the plates distorts the interface, leading to an attractive force between the two plates whose magnitude we shall now calculate. This setup has been used as a model for explaining the Cheerios effect,[1] and although we argue later that this picture is incorrect for floating objects, it does lend itself to a simple calculation. (For a further simplification leading to similar conclusions, the reader is referred to Ref. 7.)

The equation of the interface $z=h(x)$ is determined from the condition that the pressure change across the interface

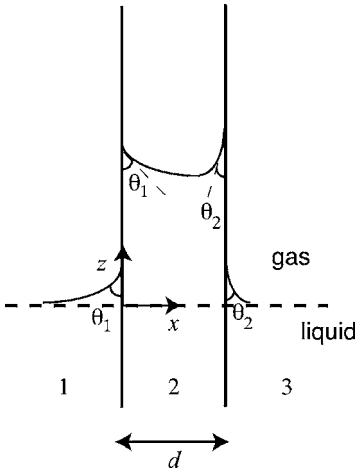

Fig. 4. The geometry of two infinite plates in a semi-infinite fluid. The planes have contact angles θ_1 and θ_2 and are at a horizontal distance d apart.

due to surface tension (which is proportional to the curvature of the interface) is equal to the hydrostatic pressure difference caused by the deformation of the interface (see Ref. 4, p. 65 for a thorough discussion). For small interfacial deflections, this balance may be written as:

$$\gamma \frac{d^2h}{dx^2} = \rho g h, \tag{1}$$

where γ is the surface tension coefficient of the liquid–gas interface, ρ is the density of the liquid, and g is the acceleration due to gravity. Equation (1) is to be solved with the boundary conditions that the contact angles, θ_1 and θ_2, are given at each of the plates and the deflection of the interface should decay far away from the plates. In the regions labeled $i=1$, 2, 3 in Fig. 4, the solution of Eq. (1) is $z=h_i(x) = A_i e^{-x/L_c} + B_i e^{x/L_c}$, where $L_c \equiv \sqrt{\gamma/\rho g}$ is the capillary length, which defines the length scale over which interactions occur. The conditions $h_1(-\infty)=0=h_3(\infty)$ give $A_1 = 0 = B_3$, which, combined with the contact angle conditions, $h_1'(0)=\cot\theta_1$ and $h_3'(d)=-\cot\theta_2$, give the interface shape outside the plates as:

$$h_1(x) = L_c \cot\theta_1 e^{x/L_c}, \tag{2}$$

$$h_3(x) = L_c \cot\theta_2 e^{(d-x)/L_c}. \tag{3}$$

The contact angle conditions, $h_2'(0)=-\cot\theta_1$ and $h_2'(d) = \cot\theta_2$, give the interface shape between the two plates:

$$\frac{h_2(x)}{L_c} = \frac{\cot\theta_1 \cosh\left(\dfrac{d-x}{L_c}\right) + \cot\theta_2 \cosh(x/L_c)}{\sinh(d/L_c)}. \tag{4}$$

Because of the interfacial deformation given by Eqs. (2)–(4), the plates are now subjected to a capillary pressure that results in a horizontal force on the plates. (There is no resultant horizontal surface tension force because its components on either side of a plate cancel exactly.) This force may act either to bring them together or to pull them apart depending on the contact angles θ_1 and θ_2. The value of the horizontal force per unit length, F_h, can be calculated by integrating

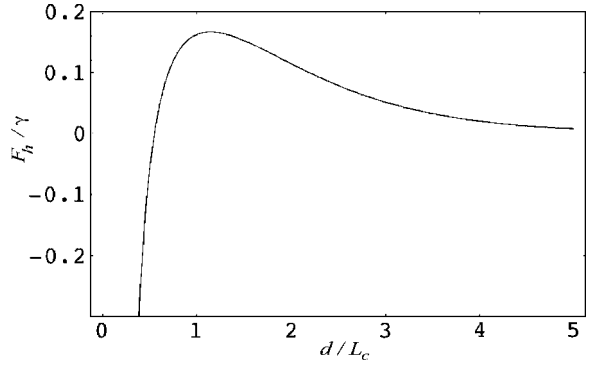

Fig. 5. A typical force-separation curve for a wetting and nonwetting plate and a liquid–gas interface. Here, $\theta_1 = 2\pi/3$ and $\theta_2 = \pi/4$, and we observe repulsion at large separations and attraction at short range.

the hydrostatic pressure along each of the wetted sides of one of the plates (say the one on the left in Fig. 4) and taking the difference as follows:

$$F_h = -\int_{-\infty}^{h_2(0)} \rho g z dz + \int_{-\infty}^{h_1(0)} \rho g z dz = \int_{h_2(0)}^{h_1(0)} \rho g z dz$$

$$= \frac{1}{2}\rho g [h_1(0)^2 - h_2(0)^2], \tag{5}$$

so that we have:

$$F_h = -\frac{\gamma}{2}\left[\frac{(\cot\theta_1 \cosh(d/L_c) + \cot\theta_2)^2}{\sinh^2(d/L_c)} - \cot^2\theta_1\right], \tag{6}$$

where the sign convention is such that $F_h<0$ corresponds to attraction between the plates. Typically this force is either attractive for all plate separations or repulsive at large separations and attractive at short separations (with an unstable equilibrium at an intermediate distance). An example of a force-displacement curve in the latter case is shown in Fig. 5.

Equation (6) can be used to show that repulsion is possible only if $\cot\theta_1 \cot\theta_2 < 0$, that is, if one plate is wetting and the other nonwetting. We note that if $\cot\theta_1 \neq -\cot\theta_2$, the fact that $F_h \to 0$ as $d \to \infty$ implies that repulsion can occur only if F_h has a maximum value somewhere, because as $d \to 0$, $F_h \to -\infty$. A simple calculation shows that the only turning point of the function $f(\xi) = (\cot\theta_1 \cosh\xi + \cot\theta_2)/\sinh\xi$ occurs at $\xi = \xi^*$, where $\cosh\xi^* = -\cot\theta_2/\cot\theta_1$, which only has a real solution ξ^* if $\cot\theta_1 \cot\theta_2 < 0$. When $\cot\theta_1 = -\cot\theta_2$, the short range attraction does not exist, and instead there is repulsion at *all* displacements. However, the result that repulsion can only occur when $\cot\theta_1 \cot\theta_2 < 0$ still stands.

This result shows that vertical plates at a liquid–gas interface will attract if they have like menisci and otherwise repel, as we saw in Sec. II with floating objects. However, the physical mechanism here is subtly different. We can no longer argue in terms of one plate following the meniscus imposed by the other because these plates do not float, meaning that there is no analogue of the condition of vertical force balance in this case. Instead, we must consider the effects of hydrostatic pressure which result from the deformation of the interface, as explained in Ref. 8 following earlier arguments by Kelvin and Tait. We give here an abbreviated version of their argument in terms of the configurations shown in Figs. 6(a) and 6(b) in which plates of like wettability are at the

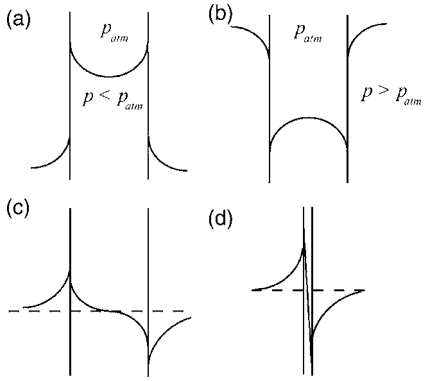

Fig. 6. Typical interfacial profiles for the different configurations of plate wettabilities. (a) Two wetting plates. (b) Two nonwetting plates. (c) A wetting and nonwetting plate at intermediate separation. (d) A wetting and nonwetting plate at short range.

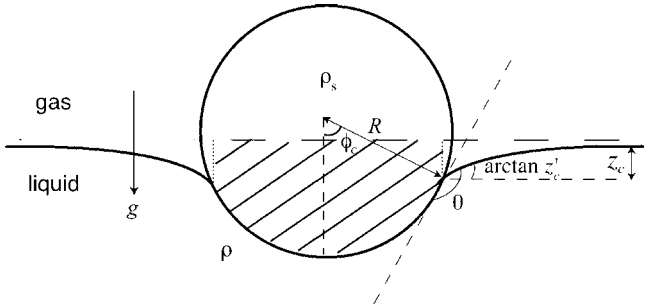

Fig. 7. Geometry of a sphere lying at a liquid–gas interface. The shaded area represents the weight of the liquid equivalent to the buoyancy force due to hydrostatic pressure acting on the sphere (Ref. 10).

interface. In Fig. 6(a), the upper portion of the central column of fluid is at a pressure lower than atmospheric pressure, p_{atm}, because of the curvature of the interface; the two plates attract because of the excess of atmospheric pressure. Similarly in Fig. 6(b), the pressure in the outer fluid is greater than p_{atm}, again because of the sign of the interfacial curvature, and so there is an excess pressure (or capillary suction) causing the two plates to attract. The situation is more complicated when one plate is wetting and the other nonwetting. At intermediate and large displacements, the interfacial displacement of the central column at the points where it touches a plate is smaller than it is on the other side of the same plate [as shown in Fig. 6(c)] due to the constraint that the central interface must pass through $z=0$ (rather than just being asymptotic to 0) to allow it to satisfy both contact angle conditions. From Eq. (5), we thus see that $F_h>0$ and so the two plates repel. When the two plates come close to contact, however, a relatively large change in the gradient of the intermediate meniscus is required between the two plates, inducing a large curvature. Because the curvature of the interface is proportional to its height, this large curvature in turn means that the displacement of the interface must be large in this region, which reverses the sign of the force and leads to attraction [see Fig. 6(d)]. The exception is the case $\cot\theta_1=-\cot\theta_2$, as noted in the discussion following Eq. (6). Here, very little curvature is required because the contact angles are precisely complementary, and so very little displacement of the interface is necessary. Thus, the interfacial displacement of the inside of the plates is smaller than that on the outside of the plates, and so, again using Eq. (5), there is mutual repulsion between the two plates, regardless of the distance between them.

This argument often has been invoked to explain the Cheerios effect (see, for example, the answer to Problem 3.100 of Walker's book[1] or do an internet search on "Cheerios effect"). Although the effects of hydrostatic pressure imbalances caused by interfacial deformation are certainly important, the calculation considered in this section cannot constitute a complete explanation because it neglects the crucial fact that Cheerios and other floating objects must satisfy a vertical force balance to be able to float. As we shall see in Sec. V, this additional requirement changes the physics fundamentally for small particles, leading to the buoyancy mechanism outlined in Sec. II providing the dominant effect. Incorporating this additional equilibrium condition, however, requires a slightly more involved calculation, which we now consider.

V. THE CASE OF FLOATING OBJECTS

Having seen the manner in which the force between two interfacial objects can be calculated in a somewhat artificial geometry, we are now in a position to consider the scenario that is of most interest to us here: interactions between objects that are *floating* at a liquid–gas interface. The major difference between the interactions between floating particles and the earlier discussion of two vertical plates is that we must now take into account the vertical force equilibrium of the object. This additional condition is actually a significant enough complication that, even using the linearized approach of Sec. IV, progress can only be made numerically. However, for sufficiently small particles we may assume that the interfacial profiles generated by one or more objects floating at the interface are sufficiently small that they may be superposed. This assumption allows us to make progress analytically.

This assumption was tacitly made in our discussion of the attraction and repulsion of objects at interfaces in Sec. II, but was first introduced by Nicolson,[3] who used it to calculate the interaction force between neighboring bubbles in bubble rafts. It was then applied to the calculation of the force between floating particles at an interface by Chan *et al.*,[9] who considered some simple illustrative particle configurations such as two horizontal cylinders floating near one another. Here we give their argument applied to the determination of the interaction force between two identical spheres floating at an interface. This application is primarily motivated by the simplicity of an experimental realization.

A. A single particle

In the spirit of the Nicolson approximation, we first neglect the presence of the second sphere and consider the vertical force balance on an isolated sphere to determine an approximate expression for the interfacial slope at the contact point, z_c' (see Fig. 7). Evaluating z_c' is equivalent to determining the value of ϕ_c, as defined in Fig. 7, because of the geometrical relation $\phi_c=\pi-\theta+\arctan z_c'$; the calculation of z_c' will prove useful for justifying Nicolson's approximation and for comparing the results with those of Sec. IV.

For the sphere to remain at the interface, its weight, $\frac{4}{3}\pi\rho_s g R^3$ must be balanced by the component of surface tension acting along the (circular) contact line and the buoy-

ancy force due to the displaced bulk fluid. The first of these forces is easily seen to be given by $2\pi R\sin\phi_c\gamma\sin(\arctan z_c')=2\pi\gamma R\sin\phi_c z_c'(1+z_c'^2)^{-1/2}$. The second is given by the weight of the water that would occupy the area between the wetted region of the sphere and the undisturbed interface, which is shown as the hatched area in Fig. 7. To understand physically this generalization of Archimedes' principle, notice that the liquid has no knowledge of the geometry of the object that is at the interface outside of its wetted perimeter. The liquid must therefore produce an upward force equal to what it would provide to an object filling the entire hatched region, which we know from the usual Archimedes result is the weight of the displaced liquid that would fill this volume. (For elegant rigorous derivations of this result, see Refs. 10 or 11.) This volume can be calculated by splitting it into a circular cylinder of radius $R\sin\phi_c$ and height z_c, and a spherical cap of height $R(1-\cos\phi_c)$ and base $R\sin\phi_c$. These considerations give the buoyancy force

$$\pi\rho g R^3\left(\frac{z_c}{R}\sin\phi_c+\frac{2}{3}-\cos\phi_c+\frac{1}{3}\cos^3\phi_c\right). \tag{7}$$

The balance of the vertical forces may now be written explicitly as:

$$\frac{4}{3}\pi\rho_s g R^3=2\pi\gamma R\sin\phi_c\frac{z_c'}{\sqrt{1+z_c'^2}}+\rho g\pi R^3\left(\frac{z_c}{R}\sin\phi_c+\frac{2}{3}-\cos\phi_c+\frac{1}{3}\cos^3\phi_c\right). \tag{8}$$

If we substitute $\phi_c=\pi-\theta+\arctan z_c'$ and keep only those terms linear in z_c', we obtain an expression for $z_c'\sin\phi_c$ accurate to first order in the *Bond number*, $B\equiv R^2/L_c^2$:

$$z_c'\sin\phi_c=B\left(\frac{2D-1}{3}-\frac{1}{2}\cos\theta+\frac{1}{6}\cos^3\theta\right)\equiv B\Sigma, \tag{9}$$

where $D\equiv\rho_s/\rho$. (As a consistency check, observe that $z_c'=0$ when $\theta=\pi/2$ and $D=1/2$, which we expect, because in this case the Archimedes buoyancy alone is enough to balance the weight of the sphere without any interfacial deformation.)

Equation (9) contains two dimensionless parameters, B and Σ. The Bond number, $B=\rho g R^2/\gamma$, is the most important dimensionless parameter in this system. It gives a measure of the relative importance of the effects of gravity and surface tension: large B corresponds to large particles or small surface tension coefficient—in both cases the surface tension is inconsequential. The expression for the slope of the interface in the vicinity of the spherical particle given in Eq. (9) is valid for $B\ll 1$ (corresponding to a radius of ~ 1 mm or smaller for a sphere at an air–water interface), in which case surface tension is very important. The other dimensionless parameter, Σ, can be thought of as a (dimensionless) resultant weight of the particle once the Archimedes force has been subtracted. This interpretation arises naturally from the vertical force balance condition (8) and (9), because the resultant weight of the object (in the linearized approximation) is $2\pi\gamma R z_c'\sin\phi_c=2\pi\gamma RB\Sigma$.

To calculate the interaction energy using the Nicolson approximation, we also must calculate the interfacial displacement caused by an isolated floating sphere, which is determined by the hydrostatic balance $\gamma\nabla^2 h=\rho g h$, the coordinate invariant statement of Eq. (1). With the assumption of cylindrical symmetry, this generalization of Eq. (1) becomes:

$$\frac{1}{r}\frac{d}{dr}\left(r\frac{dh}{dr}\right)=\frac{h}{L_c^2}, \tag{10}$$

with the boundary conditions that $h\to 0$ as $r\to\infty$ and $h'(r=R\sin\phi_c)=z_c'$. Equation (10) has a solution in terms of modified Bessel functions of the first kind[12] and of order n, $K_n(x)$:

$$h(r)=-z_c'L_c\frac{K_0(r/L_c)}{K_1(R\sin\phi_c/L_c)}\approx -z_c'\sin\phi_c R K_0(r/L_c), \tag{11}$$

where we have used the asymptotic result (see, for example, Ref. 12) that $K_1(x)\approx 1/x$ for $x\ll 1$ to simplify the prefactor.

B. Two interacting particles

Having calculated the effective weight of a sphere at a deformed interface as $2\pi\gamma RB\Sigma$ [with Σ as defined in Eq. (9)] as well as the interfacial deformation caused by the presence of a single sphere, we are now in a position to calculate the energy of interaction between two spheres. To leading order in B, this energy is the product of the resultant weight of one sphere and its vertical displacement due to the presence of another sphere with its center a horizontal distance l away. We may therefore write the energy, $E(l)$, as:

$$E(l)=-2\pi\gamma R^2B^2\Sigma^2K_0\left(\frac{l}{L_c}\right), \tag{12}$$

and from Eq. (12), the force of interaction is given by $F(l)=-dE/dl$, or:

$$F(l)=-2\pi\gamma RB^{5/2}\Sigma^2K_1\left(\frac{l}{L_c}\right). \tag{13}$$

Problem 1. Repeat the previous calculation for two cylinders of infinite length lying horizontally and parallel to one another at an interface. First consider the interfacial profile caused by an isolated cylinder and show that it is given by

$$z(x)=-L_c z_c'\exp(-x/L_c), \tag{14}$$

when $B\ll 1$. Next use the linearized vertical force balance and the geometrical relationship $\phi_c=\pi-\theta+\arctan z_c'$ to show that:

$$z_c'\approx\frac{B}{2}\left(\pi(D-1)+\theta-\frac{1}{2}\sin 2\theta\right)\equiv\frac{BC}{2}. \tag{15}$$

The resultant weight of the object can be found from the force balance to be $\approx 2\gamma z_c'$. With this effective weight and the interfacial profile in Eq. (14), calculate the energy of interaction (per unit length), $E(l)$, between two cylinders with center–center separation l. Show that

$$F(l)=-\frac{dE}{dl}=-\frac{\gamma}{2}B^2C^2\exp\left(-\frac{l}{L_c}\right), \tag{16}$$

with C defined as in Eq. (15).

It is important to emphasize that the calculation leading to Eq. (12) relies on several assumptions. The first is that the particle is small enough that the total interfacial deformation is the sum of that due to individual particles. (By comparison with numerical results, Chan *et al.*[9] show that the expression derived by their method is essentially exact for Bond numbers $B \leqslant 0.1$.) Furthermore, we have neglected the effect of capillary pressure acting on the particle to produce a horizontal force—calculated for the case of two vertical plates in Sec. IV. It is not possible using the analysis presented here to include this effect because the Nicolson approximation implicitly assumes that the level of the interface is the same on either side of the particle. However, the difference in interface heights on either side of the sphere only occurs at the next order in B, so that using Eq. (6), we see that the contribution from capillary pressure also only enters at the next order in B.

At large Bond numbers this analysis breaks down, which raises the question: is it still the case that large particles interact because of their gravitational potential energy or does the capillary suction effect discussed in Sec. IV become more important? To answer this question conclusively requires the numerical solution of the full problem, because for large Bond number the interfacial deflections are no longer small. Such a calculation is beyond the scope of this paper, but has been performed by Allain and Cloitre,[13] who showed that for $B \gg 1$, the vertical displacement of two horizontal cylinders does not change substantially as they move toward one another. Thus the attractive force must result largely from pressure effects rather than the weight of the particles, with the crossover between these two regimes occurring for $10 < B < 100$ according to the numerical results of Ref. 13.

The toroidal shape of a Cheerio complicates the notion of Bond number, but if we take the effective radius based on its volume $R^* = (R_1^2 R_2)^{1/3} \approx 2.7$ mm (where $R_1 \approx 2$ mm and $R_2 \approx 5$ mm are the two radii of the torus) and $L_c = 2.7$ mm for an air–water interface, then $B \approx 1$. This value is within the regime where the gravitational energy of the particles dominates the capillary suction due to the meniscus between them, and so it is crucial that we account for the buoyancy effects to correctly interpret the attractive force.

Finally, we discuss briefly how the result in Eq. (13) fits with the interpretation of attraction and repulsion that we developed in Sec. II. If you do Problem 2, you will see that the sign of the force between two nonidentical spheres is governed by the sign of $z_c'^{(1)} \sin \phi_c^{(1)} z_c'^{(2)} \sin \phi_c^{(2)}$, where the superscript (i) labels the two particles. The interaction is attractive if this product is positive and repulsive if it is negative. From Eq. (11) we see that this product has the same sign as the product of the gradients of the menisci in the neighborhood of the two particles, and so we see that there is mutual attraction if the particles have like menisci and repulsion if they have unlike menisci. This mathematical argument corresponds precisely to the physical picture that we saw in Sec. II, although we are now able to quantify the combination of contact angles and particle densities which gives rise to the two possibilities. We also note that the strength of the interaction decreases as the surface tension coefficient, γ, increases. This slightly counterintuitive result is a simple consequence of the fact that for higher values of γ, the deformation of the interface required to satisfy the vertical force balance condition for particle 1 is less, and so the gravitational hill on which particle 2 finds itself is smaller.

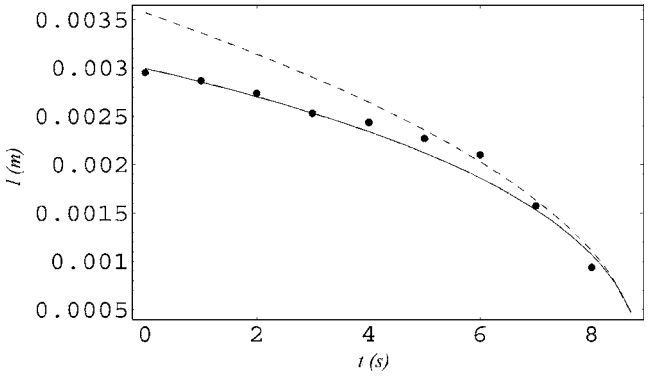

Fig. 8. Experimental data (points) compared to the solutions of the dynamical equation (17) (solid line) for two identical spheres of radius 0.3 mm interacting via flotation forces at an air–water interface. The theoretical curve is calculated by solving Eq. (17) numerically with $\gamma = 0.0728$ N m^{-1}, $\mu = 0.001$ Pa s, and $\Sigma^2/\alpha = 0.673$ used as the fitting parameter. (Σ is the dimensionless resultant weight of the spheres and α is the ratio of the drag that the particle feels at the interface to that which it would experience in an unbounded fluid.) The dashed line gives the asymptotic result (18).

Problem 2. Repeat the analysis for two spheres but now allow them to have different material properties R, θ, and D. Show that the sign of the force between two (nonidentical) spheres is determined by the sign of $z_c'^{(1)} \sin \phi_c^{(1)} z_c'^{(2)} \sin \phi_c^{(2)}$.

VI. THE DYNAMICS OF FLOATING PARTICLES

So far we have limited ourselves to calculating the force between particles. We shall now use this calculation to answer some questions that arise from observing the motion of objects at an interface. A natural question to start with is "how fast do two spherical particles come together?," a question that we shall consider in this section.

To make the dynamical problem tractable, we assume that the vertical velocity of each particle as it moves along the meniscus is small enough that the vertical force balance used to determine the horizontal force is satisfied. This assumption is valid to leading order, as shown in Ref. 9. We assume that the motion is overdamped so that a Stokes drag term[4] for the viscous drag provided by the liquid balances the attractive force between the two particles given in Eq. (13). This balance leads to the equation of motion:

$$6\pi\mu R\alpha \frac{dl}{dt} = -2\pi\gamma R B^{5/2} \Sigma^2 K_1\left(\frac{l(t)}{L_c}\right), \tag{17}$$

where μ is the dynamic viscosity of the liquid and α is a scaling factor which takes into account the fact that the drag experienced by a particle at an interface is less than it would experience if completely immersed in the bulk fluid. We expect that $\alpha \approx 1/2$, although the dependence of α on θ was computed numerically in Ref. 14. Data obtained from observing two spherical particles with radius 0.3 mm as they move under each other's influence at the interface between air and water is shown in Fig. 8. The data were collected from a time lapse video (one frame per second) of the motion

taken with a digital camcorder, which was then analyzed using image analysis software.[15] The dimensionless resultant weight of the particles, Σ, is difficult to measure experimentally because of its dependence on the contact angle θ. We thus appear to have two unknown parameters in this model (α and Σ). Fortunately, because only the ratio Σ^2/α appears in Eq. (17), we can fit the numerical solution of Eq. (17) to the experimental data presented in Fig. 8 by this one parameter.

In this case, we assume that the particles are sufficiently small that their inertia may be neglected entirely. The approach we have adopted is better suited to such small particles because the Bond number in this case also is very small, and so the expression for the interaction force in Eq. (13) is effectively exact. Also, if the typical distance between particles is small compared to the capillary length, L_c, then we again are able to use the asymptotic formula $K_1(x) \approx x^{-1}$ for $x \ll 1$ to approximate the modified Bessel function in the force law (13). We substitute this formula into Eq. (17) and solve for $l(t)$, giving:

$$l(t) \approx \sqrt{l(0)^2 - \frac{2\gamma L_c B^{5/2}\Sigma^2}{3\mu\alpha}t}, \tag{18}$$

so that the time taken for two spheres to come into contact is given by:

$$t_{\text{contact}} \approx \frac{3\mu\alpha(l(0)^2 - R^2)}{2\gamma L_c B^{5/2}\Sigma^2}. \tag{19}$$

In Fig. 8, we see that the asymptotic form (18) is a reasonable approximation over the last 2 s before contact.

To verify our assumption that the motion is slow enough for us to be able to neglect the particle's acceleration, we look at the ratio of particle inertia to Stokes drag. This ratio, $\mathcal{R}$, is initially small and increases as the particles come closer, reaching a maximum when they come in contact. If we use the asymptotic expression for $K_1(x)$, we have:

$$\mathcal{R}_{\text{contact}} = \frac{2}{27\alpha^2}\frac{\gamma\rho L_c B^{5/2}\Sigma^2}{3\mu^2}. \tag{20}$$

For spherical particles of radius less than 0.3 mm (or $B = 0.01$), $\mathcal{R} < 0.1$ throughout the motion, which is sufficiently small that our approach is self-consistent.

VII. AMPHIPHILIC STRIPS *WITHOUT* CHEMISTRY

As a final illustration of the principles that we have applied to the problem of the attraction of interfacial objects, we consider briefly the equilibrium of a single two-dimensional strip, say of plastic (of weight W per unit length into the page and width $2b$) floating horizontally at an interface, as shown in Fig. 9. This problem was studied extensively in Ref. 11, where the interactions between two such strips also was investigated. Here we content ourselves with studying the simpler problem of a single strip but with a slight twist: we take the center of mass line of the strip to be displaced from the strip's center line by a distance $(1-\beta)b$ [so that $(1-\beta)$ is a measure of the offset of the center of mass of the strip]. As we shall see, an offset center of mass is enough to break the symmetry of the problem, and thus allow the strip to float at an angle α to the horizontal.

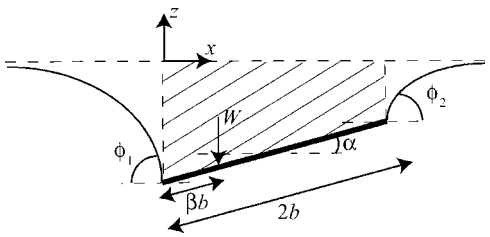

Fig. 9. A single two-dimensional strip (of weight W per unit length in the direction perpendicular to the page) floating at an interface, with the hatched area indicating the area of the displaced fluid, the weight of which is equal to the buoyancy force on the strip. The asymmetric equilibrium position here is possible because of the off-center position for the strip's center of mass.

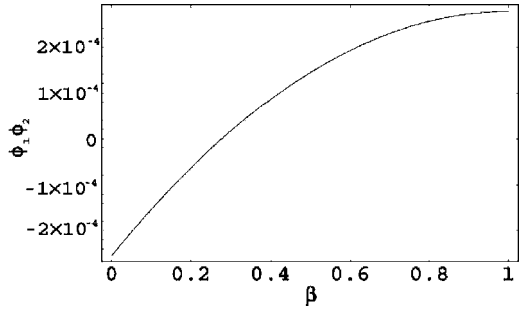

Fig. 10. The dependence of $\phi_1\phi_2$ on the offset of the strip's center of mass, given by $(1-\beta)b$, for $\beta \in [0,1]$ (the graph is symmetric about $\beta = 1$). Here the strip has dimensionless weight per unit length $W/\gamma = 0.1$ and half-width $b/L_c = 2$.

Because the strip is assumed to be infinitely thin, the concept of contact angle that we used earlier is not well-defined in this problem. Instead, the effective contact angles that the interface makes at the points of contact with the strip, $\phi_{1,2}$, and the angle α are determined from the condition that the strip be in equilibrium; this condition leads to three equations for the three unknowns. Two of these are the conditions of horizontal and vertical force balance, which we have encountered previously and may be written here as

$$0 = \gamma(\cos\phi_1 - \cos\phi_2) + \frac{\rho g}{2}(z_1^2 - z_2^2) \tag{21}$$

for horizontal equilibrium, and

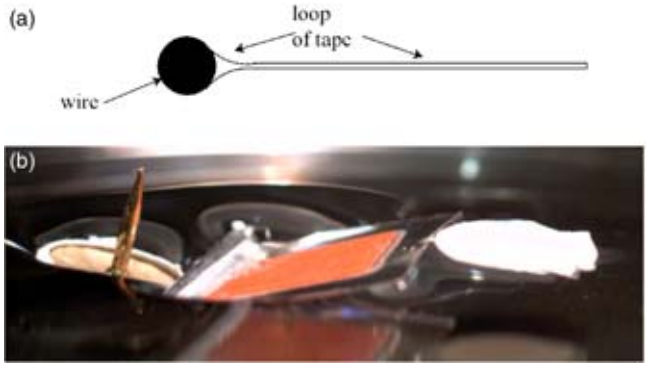

Fig. 11. Example of a simple amphiphilic strip. (a) Simple design of the amphiphilic strip discussed in the text. (b) Photograph of a realization of such an amphiphilic strip. Here the rectangular strip lies between a drawing pin (left) and the cap of another drawing pin (right). These two objects would normally be mutually repulsive (as discussed in Sec. III), but maintain a finite separation once they are separated by the amphiphile.

$$W=\gamma(\sin\phi_1+\sin\phi_2)-\rho g(2b\cos\alpha)\left(\frac{z_1+z_2}{2}\right) \tag{22}$$

for vertical equilibrium. The second term on the right-hand side of Eq. (22) is the weight of liquid displaced by the strip, which is shown as the hatched area in Fig. 9. In addition, there is the condition of torque balance, which we did not encounter for the equilibrium of the floating sphere (it is automatically satisfied for objects of circular cross-section). Here this condition is crucial because it gives a third equation by which to determine the three unknowns. By taking moments about the center of mass, we have:

$$0=\gamma b[(2-\beta)\sin(\phi_2-\alpha)-\beta\sin(\phi_1+\alpha)] - \rho g\int_{-\beta b}^{(2-\beta)b} z(s)s\,ds, \tag{23}$$

where s is an arclength coordinate measured along the strip from the center of mass.

In principle, these equations can be solved even for interfacial deformations that are not small following the strategy outlined in Ref. 11. However, for simplicity, we proceed here in the limit where the three angles are small, and, therefore, the interfacial deformations also are small. In this limit $z_1 \approx -L_c\phi_1$, $z_2\approx -L_c\phi_2$, so the vertical relation (22) becomes:

$$\frac{W}{\gamma}=(\phi_1+\phi_2)\left(1+\frac{b}{L_c}\right). \tag{24}$$

The linearized version of Eq. (21) is automatically satisfied, and so we make use of the geometrical relation $z_2-z_1=2b\sin\alpha$ to give:

$$\alpha=\frac{\phi_1-\phi_2}{2b/L_c}. \tag{25}$$

Finally, the torque balance condition (23) yields:

$$0=(2-\beta)\phi_2-\beta\phi_1-2\alpha+\frac{b}{L_c}(1-\beta)(\beta\phi_2+(2-\beta)\phi_1)+\frac{b}{L_c}\frac{\phi_2-\phi_1}{6}(\beta^3+(2-\beta)^3). \tag{26}$$

Equations (24)–(26) constitute a system of three linear equations in three unknowns, which can be solved by inverting a 3×3 matrix. Of particular interest here is the possibility that, for some values of β, ϕ_1 and ϕ_2 have opposite signs as plotted in Fig. 10. We can understand this result more by solving Eqs. (24)–(26) to give:

$$\phi_1\phi_2=\frac{W^2}{\gamma^2}L_c^2\frac{(3L_c^2+6bL_c+4b^2-3b(L_c+b)\beta)(3L_c^2-2b^2+3b(L_c+b)\beta)}{4(L_c+b)^2(b^2+3bL_c+3L_c^2)^2}. \tag{27}$$

From Eq. (27) and the restriction that $\beta\leqslant1$, it is simple to show that $\phi_1\phi_2<0$ when $\beta<\beta_c=(2b^2-3L_c^2)/[3b(b+L_c)]$, and hence ϕ_1 and ϕ_2 are of opposite sign for sufficiently small β if $b>(3/2)^{1/2}L_c$. For the parameters in Fig. 10, $\beta_c\approx0.28$, with ϕ_2 changing from negative to positive around $\beta=\beta_c$ and ϕ_1 positive for all $\beta\in[0,1]$. Physically, the change in sign of ϕ_2 is what we would expect because for small β, the offset of the center of mass causes a large torque and hence rotation of the object, forcing the far end of the strip to be displaced above the equilibrium liquid level and hence the interface here must be elevated, corresponding to $\phi_2<0$. As the offset decreases, so does the torque associated with it, and the displacement of the far end of the strip is diminished until, for sufficiently small offsets, the far end lies below the equilibrium liquid level and $\phi_2>0$.

The significance of the qualitatively different interfacial shapes at both end of the strip when $\phi_1\phi_2<0$ is that in such cases one edge is able to attract drawing pins while the other repels drawing pins and attracts bubbles! Particles or molecules with this type of behavior often are termed *amphiphiles* and occur in detergents along with many other applications.[16] However, such amphiphilic particles are usually constructed by treating the two edges chemically to induce the different behavior. Here, we have shown that this behavior also may be achieved by altering the density of the strip so that the center of mass of the object is displaced.

As well as the possible industrial applications that such particles could have, this *physical* amphiphile lends itself to a much simpler classroom demonstration than might be possible with chemical amphiphiles. By using a piece of sticky tape doubled back on itself to form the strip [see Fig. 11(a)], and a short length of wire (part of a paperclip, for example) inserted between the two sides of the tape, it is possible to make a strip with edges that deform the interface in manifestly different ways. An experimental realization is shown in Fig. 11(b), which demonstrates that particles that would otherwise be mutually repulsive can be coaxed into maintaining a finite equilibrium separation.

Fig. 12. The interfacial deformation caused by a water-spider, *Dolomedes triton*. The interface is visibly depressed by the spider's weight acting on each leg. Image courtesy of Robert B. Suter.

VIII. DISCUSSION

We have investigated an aspect of everyday life that may previously have escaped many readers' notice—the propensity of floating objects to aggregate. We expressed the mechanism for this effect in terms of the simple physics of particles trapped at a deformed interface feeling the effects of their weight (or buoyancy), and then showed how approximate methods can lead to quantitative descriptions of the magnitude and dynamical nature of the interaction. We now conclude with a brief discussion of some of the scenarios in which this effect has been applied and mention some potential research directions.

There are likely many instances where a variant of the Cheerios effect is used by one species or another. Here we choose to highlight water walking creatures that can be found on the surface of many ponds. These creatures rely on surface tension to prevent them from drowning because their weight can be supported by interfacial deformations (as shown in Fig. 12). However, when they try to climb out of the pond, they become reluctant victims of the Cheerios effect, because this action generally requires climbing up the meniscus against gravity. Recent observations[17] suggest that some insects, such as *Mniovelia Kuscheli*, can overcome this difficulty by pulling up on the interface with their front legs and pushing down on it with their hind legs, effectively shifting their center of gravity. They thus become a natural exemplar of the mechanical amphiphile discussed in Sec. VII because they are now attracted to the wall via the Cheerios effect.

There remain many interesting questions that we have not answered in this article, many of which are amenable to investigation in the classroom or the laboratory. For example, it would be worthwhile to better understand the way in which two different types of particles that are mutually repulsive interact. With a mixture of light and heavy particles, for example, clusters of like density particles form, all things (other than the particle density) being equal. This segregation phenomenon could find many applications within science and industry. Such a study could naturally be extended by the inclusion of amphiphilic particles, which would allow the user to dictate a finite equilibrium spacing between two otherwise repulsive objects. Another example is afforded by hair on water: a flexible hair floating parallel to a planar wall might be expected to bend as it is attracted to the wall because the attractive force would be greatest for those parts of the hair closest to the wall and much less significant for those parts further away. This motion has yet to be studied experimentally or theoretically. The inspiration from the kitchen, industry, and nature is almost overwhelming.

ACKNOWLEDGMENTS

This article arose as a result of a summer studentship funded by the Heilbronn Fund of Trinity College, Cambridge (D.V.). We thank John Bush and David Hu for telling us about the meniscus-climbing insect *Mniovelia Kuscheli*, Robert Suter of Vassar College for permission to use his photograph in Fig. 12, and Pascale Aussillous for assistance with the photography in Figs. 1, 3, and 11(b). An anonymous reviewer also made many useful suggestions.

[a]Electronic mail: lm@deas.harvard.edu

[1]J. Walker, *The Flying Circus of Physics* (Wiley, New York, 1977).

[2]G. M. Whitesides and B. Grzybowski, "Self-assembly at all scales," Science **295**, 2418–2421 (2002).

[3]M. M. Nicolson, "The interaction between floating particles," Proc. Cambridge Philos. Soc. **45**, 288–295 (1949).

[4]G. K. Batchelor, *An Introduction to Fluid Dynamics* (Cambridge U.P., Cambridge, 1967).

[5]D. J. Campbell, E. R. Freidinger, J. M. Hastings, and M. K. Querns, "Spontaneous assembly of soda straws," J. Chem. Educ. **79**, 201–202 (2002).

[6]P. A. Kralchevsky and K. Nagyama, "Capillary interactions between particles bound to interfaces, liquid films and biomembranes," Adv. Colloid Interface Sci. **85**, 145–192 (2000).

[7]J. C. Maxwell, "Capillary action," in *The Scientific Papers of James Clerk Maxwell*, edited by W. D. Niven (Cambridge U.P., Cambridge, 1890), Vol. 2.

[8]J. H. Poynting and J. J. Thomson, *A University Textbook of Physics* Properties of Matter, Vol. I, revised by G. W. Todd (Griffin, London, 1947), 14th ed.

[9]D. Y. C. Chan, J. D. Henry Jr., and L. R. White, "The interaction of colloidal particles collected at a fluid interface," J. Colloid Interface Sci. **79**, 410–418 (1981).

[10]J. B. Keller, "Surface tension force on a partly submerged body," Phys. Fluids **10**, 3009–1010 (1998).

[11]E. H. Mansfield, H. R. Sepangi, and E. A. Eastwood, "Equilibrium and mutual attraction or repulsion of objects supported by surface tension," Philos. Trans. R. Soc. London, Ser. A **355**, 869–919 (1997).

[12]M. Abramowitz and I. A. Stegun, *Handbook of Mathematical Functions* (Dover, New York, 1965).

[13]C. Allain and M. Cloitre, "Interaction between particles trapped at fluid interfaces. I. Exact and asymptotic solutions for the force between two horizontal cylinders," J. Colloid Interface Sci. **157**, 261–268 (1993); II. "Free-energy analysis of the interaction between two horizontal cylinders," **157**, 269–277 (1993).

[14]K. D. Danov, R. Dimova, and B. Pouligny, "Viscous drag of a solid sphere straddling a spherical or flat interface," Phys. Fluids **12**, 2711–2722 (2000).

[15]The images were analyzed using IMAGEJ, ⟨http://rsb.info.nih.gov/ij/⟩.

[16]T. Ondarçuhu, P. Fabre, E. Raphaël, and M. Veyssié, "Specific properties of amphiphilic particles at fluid interfaces," J. Phys. (Paris) **51**, 1527–1536 (1990).

[17]David Hu's website at ⟨http://www-math.mit.edu/ dhu/Videoweb/2top.mov⟩ has movies showing *Mniovelia Kuscheli* performing this trick.